COAL PILLAR'S BREAKING AND FRACTURE DEVELOPMENT
Mechanism and Numerical Simulation

by

Fei TENG[a], Minggao YU[a,b*] , Jiangkun CHAO[a], and Zhihui MA[a]

[a] School of Safety Science and Engineering, Henan Polytechnic University, Jiaozuo, China
[b] State Key Laboratory of Coal Mine Disaster Dynamics and Control,
Chongqing University, Chongqing, China

Original scientific paper
https://doi.org/10.2298/TSCI2203439T

This study explores the influence of a repeated mining process on an upper coal pillar in a close coal seam group. The pillar's breaking and instability processes are emphasized, and the influence of fracture development on the oxidation and spontaneous combustion of coal pillars is revealed. A numerical simulation is used to simulate the dynamic evolution characteristics of stress, displacement of the upper coal pillar, and the numerical results elucidate that the mining of the lower adjacent coal seam is a pressure relief process for the upper coal pillar. The theoretical length of the fracture along the strike of the upper coal pillar is also obtained for the upper coal pillar.

Key words: *fracture development of coal pillar, close seam group, oxidation and spontaneous combustion of coal pillar, repeated mining,*

Introduction

Coal production in coal-producing countries has constantly been threatened by the spontaneous combustion of coal [1, 2]. In Shendong, Yushen, Lingwu and other important coalfields in China, there are a large number of short-distance coal seams with a shallow buried depth of 80-240 m, and the mining coal will lead to a large area of land subsidence [3-5] and will destroy the local ecological environment. Chen, *et al.* [3] took much field monitoring and made a comparison with previous studies and acquired the evolution characteristics of dynamic subsidence parameters and surface cracks. Ju *et al.* [4] explained the formation mechanism of the surface's stepped subsidence area and predicted the surface subsidence profile after the sequent mining activity. Asadi *et al*. [5] introduced a new profile function method for the prediction of surface subsidence due to inclined coal-seam mining. The surface subsidence caused by coal mining has been seriously threatening the local ecological environment, and it is time to solve the problem scientifically.

The occurrence of coal seams, which are shallowly buried and closely distributed, makes the remaining coal in a goaf vulnerable to be affected by the mining of adjacent upper coal seams, and a leakage passage through the working face, gob and surface might be formed [6, 7]. The air leakage in the goaf greatly increases the possibility of cracks through the surface, resulting in a spontaneous coal combustion disaster [8-12]. In the mining process of

* Corresponding author, e-mail: 13333910808@126.com

shallow and close seam groups, the stability of the coal pillar [13] in the upper coal seam will be affected by mining disturbances in the next adjacent layer and will be in a state of dynamic balance or even fracture instability. Pan *et al.* [14] obtained the characteristics of temperature rise and oxidation of the coal body in different stress loadings and unloading scenarios through different load treatments of experimental coal samples, but the breaking and mechanism and instability processes of the coal pillar were not theoretically researched.

Based on the special occurrence conditions of repeated mining of shallow buried and close-distance coal seams in the Bulianta Coal Mine, this paper will use numerical simulation software to simulate the dynamic excavation process in the mine, and explore the fracture development and breaking mechanism of the upper coal pillar in the repeated mining process.

Numerical model and parameter setting

Model establishment

The physical model is established in accordance with the 22301 working face drilling histogram of the Bulianta Coal Mine. The primary 1-2 coal seam, fig. 1, has a depth of 162 m, a coal thickness of 5.5 m, and a mining height of 4 m. Below the 1-2 coal seam (30 m) is the 2-2 coal seam, with a 6.2 m thickness of underlying coal seam and a mining height of 5 m. There are three mining faces (A-D) with lengths of 300 m and face C with a length of 400 m. Additionally, 100~200 m of coal remained on both sides of the boundary tunnel to avoid the boundary effect. The mining is conducted according to the order of the mining faces (A-D). There is a 40 m wide coal pillar (Range x: 560~600 , Y: 100~400, Z: 90~95.5) between working faces A and B, and the coal pillar of the lower coal seam is staggered with the coal pillar of the upper coal seam by 100 m. The simulated conditions of the recovery are shown in tab. 1, and the model is shown in fig. 1.

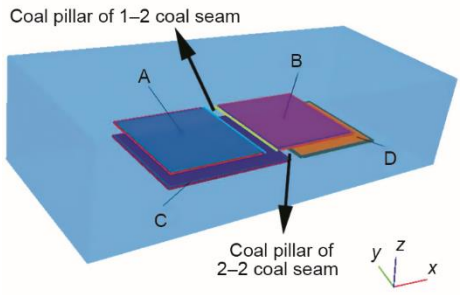

Figure 1. The coal mine excavation model

Table. 1. Simulated condition of recovery

Working face	Depth [m]	Strike length [m]	Dip length [m]	Coal thickness [m]	Mining thickness [m]
A	162	300(Y:100-400)	300(X:260-560)	5.5	4.5
B	162	300(Y:100-400)	300(X:600-900)	5.5	4.5
C	192	300(Y:100-400)	400(X:260-660)	6.2	5
D	192	300(Y:100-400)	300(X:700-1000)	6.2	5

Mechanical parameters and simulation scheme

According to the distribution of rock strata in the 22301 working face of the Bulianta Coal Mine and the field measurement of physical properties of the strata in Shendong [15], the mechanical parameters of the rock mass in each layer are determined. The Mohr Coulomb

yield criterion is adopted for model calculation, and the physical and mechanical parameters of coal and rock mass in each layer are shown in tab. 2.

Table. 2. The mechanical parameters of coal and rock

Strata	Burying depth [m]	Density [kgm^{-3}]	Modulus of elasticity [GPa]	Friction angle [°]	Cohesion [MPa]	Tensile strength [MPa]	Poisson's ratio [°]
Aeolian sand	17	1450		24.7	1.0	1.0	0.26
Sandy mudstone	124	2250	1.52	28.6	1.1	0.7	0.28
Sandy mudstone	134	2334	14.34	24.7	6.28	1.78	0.29
Coal	162	1284	1.76	23.6	17.9	1.68	0.27
Sandy mudstone	177	2308	7.27	26.1	18.96	5.24	0.26
Fine sandstone	181	2226	7.39	24.5	14.68	3.38	0.24
Sandstone	190	2185	3.88	14.1	27.6	2.88	0.27
Coal	195	1303	1.99	24.5	19.25	1.17	0.23

To analyze the dynamical evolution characteristics of stress and displacement of coal pillars in different stages of mining in shallow buried and close distance seams, the stress, displacement and plastic zone distribution of the coal body between the two faces (face A and face B) in the upper coal seam were recorded before mining, and the stress and displacement map of coal pillars in different stages was made by Surfer software after the data were derived.

Results and discussion

Stress distribution at the top surface of coal pillar in different mining stages

Figure 2 shows the *z*-direction stress distribution of the top surface of the coal pillar after the mining of working faces A-D, respectively.

When the mining face A is completed, the stress concentration is formed along the goaf side of the coal body, and the maximum stress is 8.3 MPa at the top of the coal pillar. With the increasing distance between the coal seams, the stress on the coal body is decreased. At the left boundary of the coal pillar bottom, the stress value is approximately 5.5 MPa, which is slightly increased compared with the original rock stress. There is an apparent stress concentration zone along the 570-580 m dip of the coal pillar.

When the mining face B is completed, the *z*-direction stress on the top surface of the coal pillar is basically distributed symmetrically, and the maximum stress value along the goaf on both sides of the coal pillar is approximately 10 MPa. The minimum *z*-direction stress in the middle of the core area of the coal pillar is about 7.4 MPa.

When the mining face C is completed, the coal pillar of the upper coal seam is in the disturbed fracture zone of the lower coal seam, and the mining of the lower coal seam leads to a new balance of the coal pillar of the upper coal seam. At this time, 200-300 m along the strike of the left side of the coal pillar is the place with the largest stress on the top of the whole coal pillar, and the maximum stress is approximately 4 MPa. Taking this as the center,

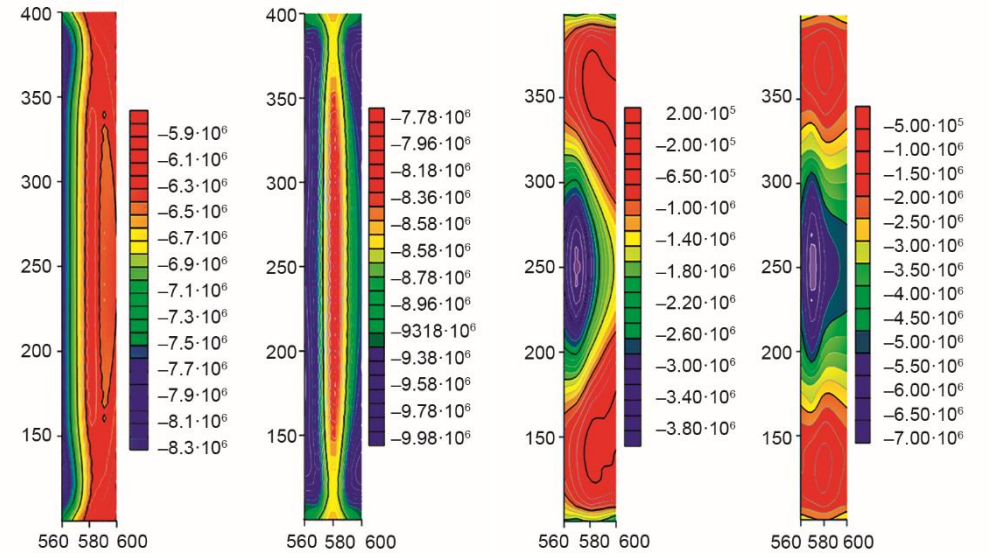

Figure 2. The *z*-direction stress distribution of the coal pillar top surface in different mining stages (completion of faces, A-D)

the absolute value of the stress decreases in an elliptical wave to the right until the stress value at the right boundary of the coal pillar reaches 1.5 MPa, and the stress direction is downward.

When the mining face D is completed, the maximum stress is 7.5 MPa on the left side of the top of coal pillar along the strike of 200-300 m. It decreases to the right and reaches approximately 5 MPa at the right boundary of coal pillar, and the stress on the top of the coal pillar increases to more than 4.5 MPa at 200-300 m along the strike. The stress on the top of the coal pillar decreases from the middle to both sides along the strike.

The z-displacement distribution at the top surface of coal pillar in different mining stages

Figure 3 shows the *z*-displacement distribution map of the top surface of the coal pillar.

When the mining face A is completed, the top surface of the coal pillar drops slightly compared with the original state, and the subsidence is approximately 0.125-0.2 m. The subsidence on the left side of the coal pillar is less than that on the right side. The subsidence on both ends of the coal pillar along the strike is greater than that in the middle. At this time, the coal pillar is in the elastic compaction stage.

When the mining face B is completed, the *z*-direction displacement of the coal pillar top is still small, between 0.28 and 0.43 m, and the *z*-direction displacement of top of the coal pillar shows the characteristics of large subsidence on both sides and small subsidence in the middle.

When the mining face C is completed, the *z*-direction displacement of the top surface of the coal pillar in the upper coal seam changes greatly due to the mining of working face C. 1) In the middle of the coal pillar, the entire coal pillar sinks approximately 3.6 m along the strike of 150-350 m, and the sinking area accounts for nearly 2/3 of the top slice of the whole coal pillar.

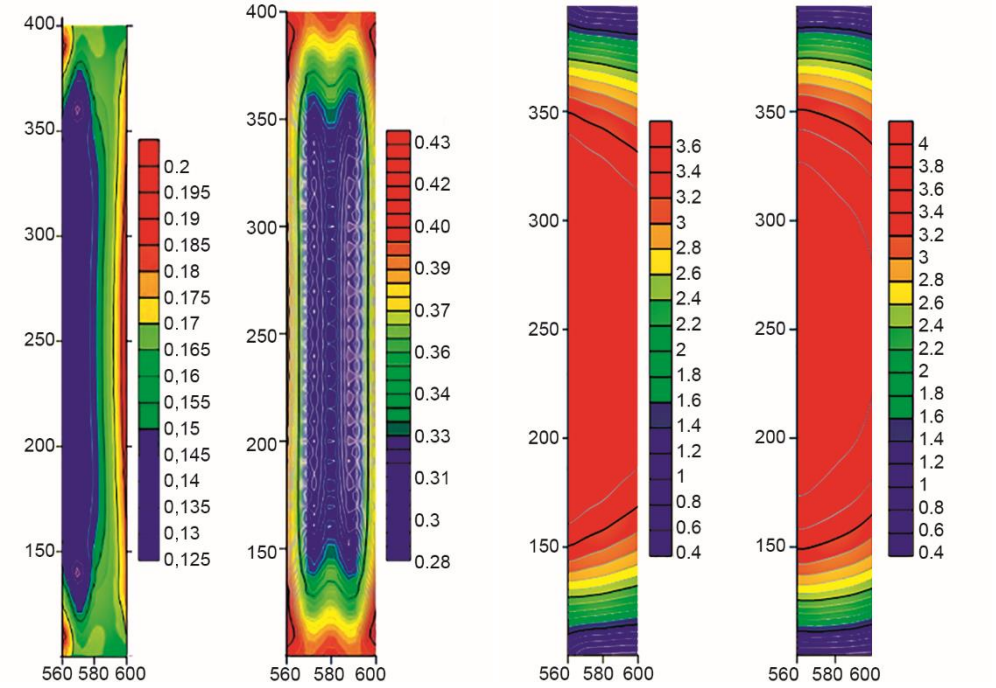

Figure 3. The *z*-direction displacement distribution on top of coal pillars in different mining stages (completion of face A-D)

After the completion of the mining face D, the *z*-direction displacement of the top of the coal pillar basically shows the same trend as the previous mining stages, with a large amount of decline along the middle of the strike and a small amount of decline on both sides. The *z*-direction displacement of the coal pillar bottom basically shows the same trend as the previous mining stages, with a large decline in the middle and a small decline on both sides along the strike. The mining face D is a stress concentration process for the coal pillar.

Breaking mechanism of coal pillar along strike

Therefore, in this paper, the authors analyze the instability mechanism of the coal pillar under the special conditions of repeated mining and staggered arrangement of coal pillars in shallow and short-distance coal seams.

It can be seen from figs. 4 and 5 that with the continuous mining of the face C, as there is no key layer between the upper and lower coal seams, when the working face advances along the strike for a certain distance, the overburden rock continues to collapse towards the goaf of face C. When the hanging length of the coal pillar in upper coal seam exceeds a certain distance, the coal pillar will break along the strike, thus forming an articulated blocks G and H. At this time, it is not the excessive load that causes the collapse and instability of the coal pillar, but the rock under the coal pillar is affected by the mining of the lower coal seam, leading to the fracture and instability of the coal pillar along the strike.

According to the above analysis, the *masonry beam* theory is used to analyze the coal pillar broken along the strike. At the moment when the coal pillar starts to break, the mechanical model shown in fig. 6 is established for the key block G. Among them, F_B is the sup-

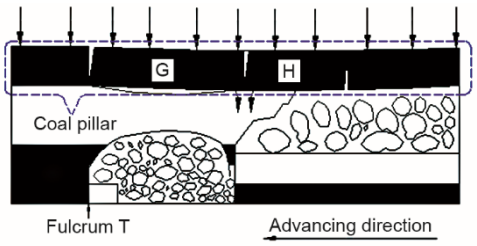

Figure 4. Section of the coal pillar along the trend at the stage of C recovery

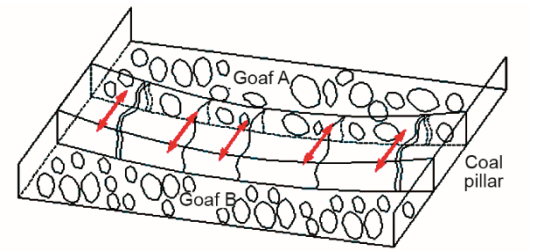

Figure 5. Fracture and instability diagram of coal pillar along strike

porting force of the coal pillar floor bedrock to coal pillar fracture block G. According to the moment balance relationship, it can be solved:

$$F_B = \frac{1}{k_b}\left(R_H + \frac{1}{2}ql_g\right) \tag{1}$$

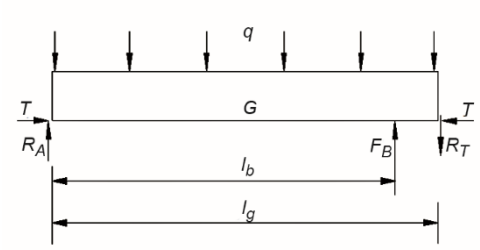

Figure 6. Mechanical model of broken coal G column

where l_g is the length of the broken coal body G, R_H – the shear stress of the hinge between the broken coal bodies G and H, q – the load on the coal pillar, k_b – the coefficient, $k_b = l_b/l_g$, and l_b – the strike distance of the supporting force F_B relative to the broken coal body boundary T.

According to the theoretical calculation model of the *block structure of voussoir beam* [15-17] with overburden broken, we obtain:

$$R_H = \frac{4h_1 - 3l_1\sin\alpha}{2(2h_1 - l_1\sin\alpha)}ql_1 \tag{2}$$

where l_1 is the length of the broken coal pillar, h_1 – the width of the broken coal pillar, and α – the rotation angle of the broken coal rock mass H. Therefore, eq. (2) can be expressed:

$$F_B = \frac{l_g}{l_b}\left(\frac{18 - 3l_1\sin\alpha}{18 - 2l_1\sin\alpha}ql_1 + \frac{1}{2}ql_g\right) \tag{3}$$

Then, the expression of l_1 is obtained:

$$l_1 = \frac{2k\sin\alpha + 18q + \sqrt{4k^2\sin^2\alpha + 342q^2 - 114k\sin\alpha}}{69\sin\alpha} \tag{4}$$

In this paper, calculated by eq. (4), the ultimate breaking length, l_1, of the coal pillar along the strike is 54.75 m under simulated working conditions. Combined with the stress displacement distribution map of the coal pillar after the completion of the face C, it can be seen that the position 40-60 m away from the two ends of the coal pillar along the strike is the place where the stress increases sharply and the z-direction displacement increases abruptly.

Combined with the *z*-direction displacement of coal pillar in different stages of mining, it can be well explained that when the coal pillar is staggered outside, mining the adjacent coal seam below will make the upper coal pillar sink step by step, which will lead to the relative cutting of coal pillar along the strike.

Discussion and conclusions

This paper uses numerical simulation software to simulate the repeated mining process of shallow buried and close-seam groups. Hinted by recent publications by Zuo and Liu [18, 19], we thought that the fractal calculus and fractional calculus are the future frontiers [20-25] might be an effective tool to the treatment of the fracture property. The pillar's stress-strain relationship can be obtained by the dimensional analysis as those in [26, 27]. The pillar's reliability can be studied using the polynomial chaos expansion method [28].

The conclusions are as follows.

- In the process of repeated mining of the close coal seam group, the mining of the lower adjacent layer is a pressure relief process for the upper coal pillar. The main reason for the instability of the upper coal pillar is the different distribution of the stress caused by the mining of the lower coal seam.
- The numerical simulation and data analysis show the fracturing mode of the coal pillar along the strike in the upper coal seam vividly. The "masonry beam" is used to calculate the ultimate fracture length of the coal pillar along the strike under this working condition, which is consistent with the numerical simulation results.

Acknowledgment

This work was financially supported by the research fund provided by the National Key Research and Development Program of China (2018YFC0807900), the National Scientific Foundation of China (51774115).

References

[1] Genc, B., Cook, A., Spontaneous Combustion risk in South African Coalfields, *Journal of South African Institute of Mining and Metallurgy, 115* (2015), 7, pp. 563-568
[2] Wactawik, J., A Numerical Simulation of Spontaneous Combustion of Coal in Goaf, *Fuel and Energy Abstracts, 39* (1998), 1, pp. 15-19
[3] Chen, C., *et al.*, Dynamic Surface Subsidence Characteristics due to Super-Large Working Face in Fragile-Ecological Mining Areas: A Case Study in Shendong Coalfield, China, *Advances in Civil Engineering, 2019* (2019), ID 8658753
[4] Ju, J. F., *et al.*, Surface Stepped Subsidence Related to Top-Coal Caving Longwall Mining of Extremely Thick Coal Seam Under Shallow Cover, *Int. J. Rock. Mech. Min., 78* (2015), C, pp. 27-35
[5] Asadi, A., *et al.*, Development of a New Mathematical Model for Prediction of Surface Subsidence Due to Inclined Coal-Seam Mining, *Journal of South African Institute of Mining and Metallurgy., 105* (2005), 1, pp. 15-20
[6] Xie, H., *et al.*, Application of FLAC to Predict Ground Surface Displacements due to Coal Extraction and Its Comparative Analysis, *Chinese Journal of Rock Mechanics And Engineering, 5* (1999), 4, pp. 29-33
[7] Si, L. L., *et al.*, Modeling and Experiment for Effective Diffusion Coefficient of Gas in Water-Saturated Coal, *Fuel, 284* (2021), Jan., 118887
[8] Guo, H., *et al.*, Mining-Induced Strata Stress Changes, Fractures and Gas Flow Dynamics in Multi-Seam Longwall Mining, *Int. J. Rock. Mech. Min., 54* (2012), Sept., pp. 129-139
[9] Chao, J. K., *et al.*, An Experimental Study on the Oxidation Kinetics Characterization of Broken Coal Under Stress Loading, *Fuel, 287* (2021), Mar., 119515
[10] Majdi, A., *et al.*, An Estimation of the Height of Fracture Zone in Longwall Coal Mining, *Journal of the American Chemical Society., 107* (2012), 14, pp. 4343-4345

[11] Ban, T., *et al.*, He's homotopy Perturbation Method for Solving Time Fractional Swift- Hohenberg Equations, *Thermal Science*, *22* (2018), 4, pp. 1601-1605
[12] Ban, T., *et al.*, Effect of Ignition Energy on Coal Dust Explosion, *Thermal Science*, *24* (2020), 4, pp. 2621-2628
[13] Hao, M., *et al.*, Hazardous Areas Determination of Coal Spontaneous Combustion in Shallow-Buried Gobs of Coal Seam Group: A Physical Simulation Experimental Study, *Environmental Earth Sciences*, *78* (2019), 39, pp. 1-11
[14] Pan, R., *et al.*, Oxidation Characteristics of Unloaded Coal Under Different Initial Stress, *Journal of China Coal Society*, *42* (2017), 9, pp. 2369-2375
[15] Li, H., *et al.*, Physical and Mechanical Properties of the Coal-Bearing Strata Rock in Shendong Coal Field, *Journal of China Coal Society*., *41* (2016), 11, pp. 2661-2671
[16] He, C. C., Xu, J. L., Subsidence Prediction of Overburden Strata and Surface Based on the Voussoir Beam Structure Theory, *Advances in Civil Engineering*, *2018* (2018), ID 2606108
[17] Zhu, L., *et al.*, The Effects of the Rotational Speed of Voussoir Beam Structures Formed by Key Strata on the Ground Pressure of Stopes, *International Journal of Rock Mechanics and Mining Sciences*, *108* (2018), Aug., pp. 67-79
[18] Zuo, Y.-T., Liu, H.-J., Fractal Approach to Mechanical and Electrical Properties of Graphene/Sic Composites, *Facta Universitatis-Series Mechanical Engineering*, *19* (2021), 2, pp. 271-284
[19] Zuo, Y.-T., A Gecko-Like Fractal Receptor of a Three-Dimensional Printing Technology: A Fractal Oscillator, *Journal of Mathematical Chemistry*, *59* (2021), Jan., pp. 735-744
[20] Tian, D., *et al.*, Fractal N/MEMS: From Pull-In Instability to Pull-In Stability, *Fractals*, *29* (2021), 2, 2150030
[21] Tian, D., He, C. H., A Fractal Micro-Electromechanical System and its Pull-In Stability, *Journal of Low Frequency Noise Vibration and Active Control*, *40* (2021), 3, pp. 1380-1386
[22] Wang, K. L., He, C. H., A Remark on Wang's Fractal Variational Principle, *Fractals*, *27* (2019), 8, 1950134
[23] Wang, K. L., *et al.*, Physical Insight of Local Fractional Calculus and Its Application to Fractional KdV-Burgers-Kuramoto Equation, Fractals, *27* (2019), 7, 1950122
[24] He, J. H., *et al.*, Variational Approach to Fractal Solitary Waves, *Fractals*, *29* (2021), 7, 2150199
[25] Tian, Y., Liu, J., Direct Algebraic Method for Solving Fractional Fokas Equation, *Thermal Science*, *25* (2021), 3, pp. 2235-2244
[26] He, C. H., *et al.* A Novel Bond Stress-Slip Model for 3-D Printed Concretes, *Discrete and Continuous Dynamical Systems Series S*, *15*, (2022), 7, pp. 1669-1683
[27] Estrada-Diaz, J. A., *et al.*, A Mathematical Dimensionless Model for Electrohydrodynamics, *Results in Physics*, *25* (2021), June, 10425
[28] Li, Y. T., *et al.*, Failure Correlation Reliability Analysis of Solid Rocket Motor Grain Based on Polynomial Chaos Expansion, *Journal of Mechanical Science and Technology*, *34* (2020), 8, pp. 3189-3195

Paper submitted: May 1, 2020
Paper revised: Oct. 4, 2021
Paper accepted: Oct 4, 2021